

**Solar Energy Conversion at
Dye Sensitized Nanostructured
Electrodes Fabricated by
Sol-Gel Processing**

Final Report

DISTRIBUTION OF THIS DOCUMENT IS UNLIMITED
ph

P.C. Searson and G.J. Meyer
*The Johns Hopkins University
Baltimore, Maryland*

MASTER

NREL technical monitor: R. McConnell



National Renewable Energy Laboratory
1617 Cole Boulevard
Golden, Colorado 80401-3393
A national laboratory of
the U.S. Department of Energy
Managed by Midwest Research Institute
for the U.S. Department of Energy
under Contract No. DE-AC36-83CH10093

Prepared under Subcontract No. XAD-3-12114-04
July 1998

This publication was reproduced from the best available camera-ready copy submitted by the subcontractor and received no editorial review at NREL.

NOTICE

This report was prepared as an account of work sponsored by an agency of the United States government. Neither the United States government nor any agency thereof, nor any of their employees, makes any warranty, express or implied, or assumes any legal liability or responsibility for the accuracy, completeness, or usefulness of any information, apparatus, product, or process disclosed, or represents that its use would not infringe privately owned rights. Reference herein to any specific commercial product, process, or service by trade name, trademark, manufacturer, or otherwise does not necessarily constitute or imply its endorsement, recommendation, or favoring by the United States government or any agency thereof. The views and opinions of authors expressed herein do not necessarily state or reflect those of the United States government or any agency thereof.

Available to DOE and DOE contractors from:

Office of Scientific and Technical Information (OSTI)
P.O. Box 62
Oak Ridge, TN 37831

Prices available by calling (423) 576-8401

Available to the public from:

National Technical Information Service (NTIS)
U.S. Department of Commerce
5285 Port Royal Road
Springfield, VA 22161
(703) 487-4650



DISCLAIMER

**Portions of this document may be illegible
electronic image products. Images are
produced from the best available original
document.**

FINAL REPORT

Solar Energy Conversion at Dye Sensitized Nanostructured Electrodes Fabricated by Sol-Gel Processing

(XAD-3-12114-04)

Principle Investigators:

P.C. Searson and G.J. Meyer

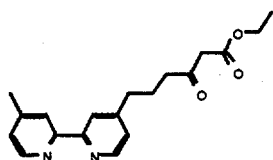
The Johns Hopkins University, Baltimore, MD 21218

Introduction

The significant achievements accomplished in this program include: 1) the first demonstration of osmium polypyridyl compounds as sensitizers; 2) the first demonstration of donor-acceptor compounds as sensitizers; 3) the first utilization of alternative acac based sensitizer-semiconductor linkages; 4) the first demonstration of "remote" interfacial electron transfer; 5) the first application of bimetallic compounds as sensitizers; 6) the first correlation of the interfacial charge recombination rate constant with the open circuit photovoltage in sensitized materials; 7) the first demonstration of a solid state dye sensitized TiO₂ cell; 8) an alternative band edge unpinning model for the nanocrystalline TiO₂/electrolyte interface at negative applied potentials; and 9) the first self-consistent model of electron transport in dye sensitized TiO₂ films. In the following sections we summarize some of the results from this program and highlight the key findings.

Novel Molecular Sensitizers and Interfacial Electron Transfer Kinetics

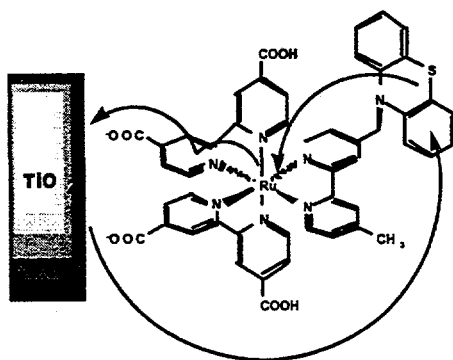
Sensitization of TiO₂ materials to visible light occurs most efficiently and effectively with Ru^{II} polypyridyl compounds as molecular sensitizers [1]. Electron transfer from the metal-to-ligand charge transfer (MLCT) excited states to the TiO₂ material forms an interfacial charge separated pair, [TiO₂(e⁻)-Ru^{III}]. Forward electron transfer rates from the MLCT excited states of Ru(dcb)(bpy)₂²⁺ (where dcb is 4,4'-(COOH)₂-2,2'-bipyridine) and related sensitizers anchored to TiO₂ were quantified, with some assumptions, by picosecond photoluminescence measurements [2]. The data are well described by a log-normal distribution of interfacial electron transfer rates with peak amplitude $\sim 10^9 - 10^{10} \text{ s}^{-1}$. Back electron transfer from TiO₂ to the *t*_{2g} orbitals of the Ru^{III} center was initially explored by time resolved diffuse reflectance spectroscopy [3]. Interfacial electron transfer occurred on a microsecond time scale and could be fit to a single exponential process, $k_r = 3 \pm 2 \times 10^6 \text{ s}^{-1}$. More recently we have prepared transparent sol-gel processed TiO₂ colloids, films, and membranes that allow spectroscopic measurements to be performed in a transmission mode. With a much improved signal to noise ratio, the kinetics are non-exponential but well described by a sum or a skewed distribution of first order rate constants. Average rate constants abstracted from these models do agree well with the diffuse reflectance measurements [4].



We recently reported the preparation, spectroscopic, surface attachment, and photoelectrochemical properties of a Ru^{II} compound coordinated to a 2,2'-bipyridine ligand with a pendant acac derivative (abbreviated bpy-acac), shown on the left [5]. The compound Ru(dmb)₂(bpy-acac)²⁺, dmb is 4,4'-(CH₃)₂-2,2'-bipyridine, was prepared and anchored to sol-gel processed TiO₂ and ZrO₂ nanostructured films. Surface attachment was well described by the Langmuir adsorption isotherm model that allows an adduct formation constants to be abstracted. The surface coverage was about a factor of three lower than that measured for related sensitizers based on carboxylic acid groups. The rate of electron injection from Ru(dmb)₂(bpy-acac)^{2+*} to TiO₂ was faster than we could time resolve with our apparatus, $k_{et} > 5 \times 10^7 \text{ s}^{-1}$. Back electron transfer to ground state products was well described by the Kohlrausch-Williams-Watts model which yields a mean rate constant of $9.62 \pm 0.77 \times 10^4 \text{ s}^{-1}$. An important

finding from these studies is that intimate electronic communication between the surface binding group and the chromophoric ligand is not a strict requirement for efficient interfacial charge separation [5].

The attachment of the donor-acceptor compound $\text{Ru}(\text{dcb})_2(4\text{-CH}_3,4'\text{-CH}_2\text{-PTZ,-bpy})]^{2+}$, where PTZ is phenothiazine, to TiO_2 represents our initial effort to control regeneration of the oxidized sensitizer by intramolecular electron transfer [6]. The strategy in the design of this

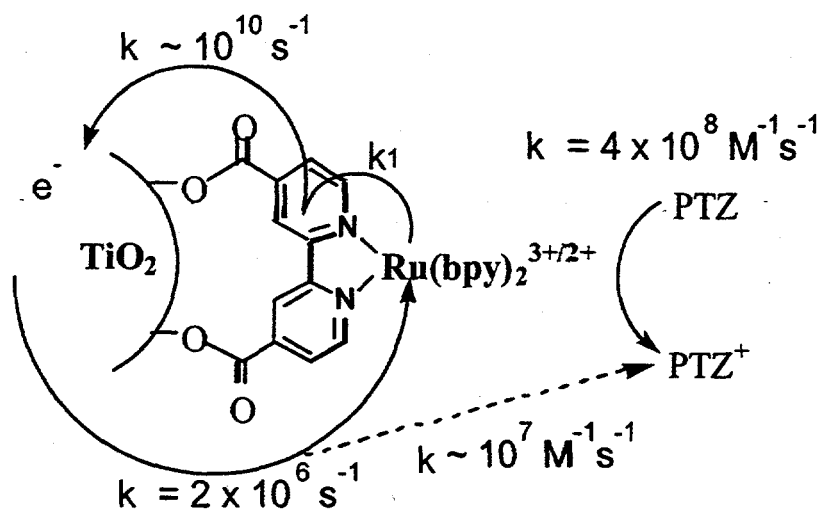


compound was as follows. A visible photon creates the MLCT excited state that rapidly and efficiently injects an electron into TiO_2 . It is then thermodynamically downhill for the pendant PTZ group to reduce the $\text{Ru}(\text{III})$ center by ~ 600 mV. The net effect is an interfacial charge separated pair with an electron in TiO_2 and the hole on PTZ abbreviated $[\text{TiO}_2(e^-)|\text{-Ru}(\text{II})\text{-PTZ}^+]$. The hope was that by translating the hole from the metal center to the PTZ group the electronic coupling to the

surface would decrease and the back reaction slowed down. This expectation was realized. The interfacial charge separated state $[\text{TiO}_2(e^-)|\text{-Ru}(\text{II})\text{-PTZ}^+]$ recombines to ground state products on a millisecond time scale, $k_r = 3.6 \times 10^3 \text{ s}^{-1}$ in propylene carbonate. This is approximately three orders of magnitude slower than a model compound, $\text{Ru}(\text{dcb})_2(\text{dmb})^{2+}$, that does not contain the pendant PTZ group. Furthermore, the measured recombination kinetics directly predict the increased open circuit voltage measured in a regenerative solar cell when compared to a model compound. Remarkably, these materials behave like ideal diodes over 5 decades of irradiance! Our ability to relate molecular recombination kinetics to the voltage output in a regenerative solar cell is unprecedented. The strategy of hole translation by intramolecular electron transfer was successful and can be applied to other molecular assemblies to prevent charge recombination and increase solar conversion efficiencies.

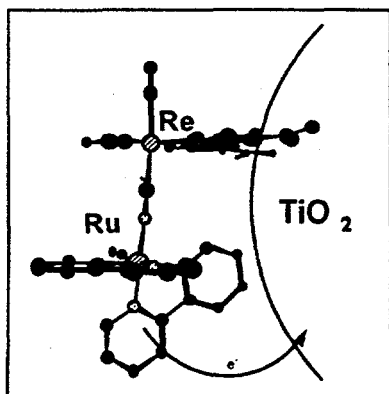
These studies were extended to interfacial charge separation with a related assembly that consists of $\text{Ru}(\text{dcb})(\text{dmb})_2^{2+}/\text{TiO}_2$ with PTZ derivatives in fluid solution [7]. To help bridge the gap between colloidal solutions and nanocrystalline films, both were explored. Through a

combination of transient absorption and luminescence spectroscopies we have been able to quantify the electron transfer dynamics shown schematically below. In these materials, hole transfer from the surface bound $\text{Ru}^{\text{III}}(\text{dcb})(\text{dmb})_2^{3+}$ center to a PTZ derivative in fluid solution was time resolved and occurred with approximately the same rate for both colloidal solutions and films, $k = 3.6 \pm 0.6 \times 10^8 \text{ M}^{-1}\text{s}^{-1}$. Significantly, the phenothiazines were able to reduce all the oxidized sensitizers on the TiO_2 surfaces within experimental error. In colloidal solutions the charge separated pairs, $[\text{TiO}_2(\text{e}^-)\text{-Ru}^{\text{III}}, \text{PTZ}^+]$, recombine on a notably long time



scale, $k = 1.3 \pm 0.3 \times 10^7 \text{ M}^{-1}\text{s}^{-1}$. The corresponding process in colloidal films also follows second-order equal-concentration kinetics however, the relevant path length is unknown and the corresponding second-order rate constant is less certain. Regardless of the actual rate constant, the high local concentrations present in the colloidal film result in a much shorter lifetime for charge separated pairs.

In an effort to achieve improved molecular control of sensitizer orientation bimetallic coordination compounds based on rhenium and ruthenium were employed. The bimetallic compounds $[(\text{dcb})\text{Re}^{\text{I}}(\text{CO})_3\text{-CN-Ru}^{\text{II}}(\text{bpy})_2(\text{CN})](\text{PF}_6)$ and the linkage isomer $[(\text{dcb})\text{Re}^{\text{I}}(\text{CO})_3\text{-NC-Ru}^{\text{II}}(\text{bpy})_2(\text{CN})](\text{PF}_6)$, were prepared, characterized, and anchored to sol-gel processed nanocrystalline TiO_2 and ZrO_2 surfaces [8]. The facial geometry about the Re^{I} center orientates the Ru^{II} center proximate to the TiO_2 surface as is shown. Long wavelength excitation is



absorbed almost exclusively by the $-\text{Ru}^{\text{II}}(\text{bpy})_2$ group.

Photoelectrochemical and time resolved absorption measurements demonstrate that rapid and efficient interfacial electron transfer and a remarkably high light-to-electrical energy conversion can be realized even though the chromophoric unit is remote to the semiconductor-bound ligand. An important implication from this conclusion is that chromophores bound to

TiO_2 through non-chromophoric ligands or non-covalently may also efficiently separate charge. Further, back electron transfer to ground state products was slowed down by approximately a factor of two when compared to *cis*- $\text{Ru}(\text{dcb})_2(\text{CN})_2$ anchored to TiO_2 and measured under the same conditions [9]. This observation suggests that an as-of-yet undetermined optimal sensitizer-surface orientation exists, wherein charge separation is still efficient but, the back reaction is further inhibited.

We have made considerable progress in the development of black $\text{Ru}(\text{II})$ polypyridyl complexes for this application. For ruthenium diimine compounds, the metal-to-ligand charge transfer (MLCT) absorption can be extended to longer wavelengths by appropriate substituent changes on chromophoric ligands or by decreasing the $d\pi-\pi^*$ back bonding donation to non-chromophoric ligands. In our initial studies, we employed the former approach and utilized diimine ligands substituted in the 5,5'-positions that have lower π^* accepting orbitals than the commonly utilized 4,4'-(COOH)₂-2,2'-bipyridine, dcb. With this ligand we prepared a family of compounds of the general form *cis*- $\text{Ru}(5,5'\text{-dcb})_2\text{X}_2$ where X is Cl^- , CN^- , and NCS^- , and contrasted the photophysical and photoelectrochemical properties with the analogous sensitizers based on dcb. While some spectral enhancement was observed, the sensitizers did not perform as efficiently as those based on dcb. Photoelectrochemical and photophysical measurements indicated that the decreased solar conversion efficiency was largely due to a lower quantum yield for interfacial charge separation [10]. The results indicate that these sensitizers would be more efficient with a semiconductor material that has a more positive conduction band edge, tin oxide for example.

An alternative approach to increase spectral response is to utilize metals other than ruthenium. While our proposed studies with Fe(II) and Cu(I) chromophores have thus far been unsuccessful, we have achieved broad spectral response with *cis*-Os(dcb)₂(CN)₂. This complex sensitizes TiO₂ to wavelengths longer than 700 nm [11]. The photocurrent response at short wavelengths is not as high as that observed for the analogous Ru(II) sensitizer. Diffuse reflectance and transient absorption measurements demonstrate that the lower photocurrent efficiency stems from less efficient iodide oxidation [12]. To achieve high photocurrent production with Os(II) polypyridyl sensitizers alternative strategies must be adopted to enhance donor oxidation efficiencies. Stronger reducing agents as electrolyte donors or sensitizers with more positive Os^{III/II} reduction potentials will produce higher photocurrents. Studies of this type, could lead to efficient semiconductor sensitization by Os(II) transition metal complexes.

References

1. B.O'Regan and M. Gratzel, *Nature* 353, 737 (1991).
2. T.A. Heimer, and G.J. Meyer, *J. Lumin.* 70, 468 (1996).
3. T.A. Heimer, and G.J. Meyer, *Proc.-Electrochem. Soc.* 121, 167 (1995).
4. J.M. Stipkala, T.A. Heimer, K.J.T. Livi, and G.J. Meyer, *Chem. Mater.* 9, 2341 (1997).
5. T.A. Heimer, S.T. D'Arcangelis, F. Farzad, J.M. Stipkala, and G.J. Meyer, *Inorg. Chem.* 35, 5319 (1996).
6. R. Argazzi, C.A. Bignozzi, T.A. Heimer, F.N. Castellano, and G.J. Meyer, *J. Am. Chem. Soc.* 117, 11815 (1995).
7. R. Argazzi, C.A. Bignozzi, T.A. Heimer, F.N. Castellano, and G.J. Meyer, *J. Phys. Chem. B* 2591 (1997).
8. R. Argazzi, C.A. Bignozzi, T.A. Heimer, and G.J. Meyer, *Inorg. Chem.* 36, 2 (1997).
9. G.M. Hasselmann, work in progress.
10. R. Argazzi, C.A. Bignozzi, T.A. Heimer, and G.J. Meyer, *Inorg. Chem.* 33, 5741 (1994).
11. T.A. Heimer, C.A. Bignozzi, and G.J. Meyer, *J. Phys. Chem.* 97, 11987 (1993).
12. T.A. Heimer, and G.J. Meyer, *Proc.-Electrochem. Soc.* 121, 187 (1995).

A Solid State, Dye Sensitized Photoelectrochemical Cell

We have achieved one of the first demonstrations of a solid state, dye sensitized photoelectrochemical cell using a polymer gel electrolyte. A typical example of an electrolyte composition was 1.4 g of polyacrylonitrile, 10 g of ethylene carbonate, 5 ml of propylene carbonate, 5 ml of acetonitrile, 1.5 g of NaI and 0.1 g of I₂. The electrolyte was solution cast onto the dye-coated TiO₂ film and pressed together with a platinum coated ITO counter electrode under N₂ atmosphere in a glove box.

Figure 1 shows current - voltage curves for a cell with the polymer gel electrolyte in the dark and under white light illumination at an intensity of 30 mW cm⁻². The current - voltage curves were obtained at a scan rate of 5 mV s⁻¹ in a two electrode arrangement. The short circuit current for the cell, shown in Figure 1, is 3.4 mA cm⁻² and the open circuit voltage is 0.58 V, comparable to cells with a liquid electrolyte. The fill factor is 0.67 giving an overall energy conversion efficiency of 4.4 %. Identical results were obtained from current - voltage curves recorded by varying an external load resistor. The dark current-voltage curve shows a very small anodic current in the potential range of the photocurrent plateau and the onset of a cathodic current at about -0.4 V, presumably due to iodine reduction.

Figure 2 shows the incident photon-to-current conversion efficiency (IPCE) versus wavelength for the polymer gel electrolyte cell. The photocurrent spectrum is relatively broad, characteristic of the 4,4'-(dcb)₂Ru(SCN)₂ dye absorption spectrum. The IPCE exhibits a peak at 540 nm with a maximum of 37%, about a factor of 2 lower than the values usually obtained for cells with a liquid electrolyte.

In summary, we have fabricated a dye sensitized porous TiO₂ photoelectrochemical cell with a polymer gel electrolyte. These cells exhibit open circuit voltages and fill factors comparable with liquid electrolyte cells and have an energy conversion efficiency of 3-5 % under white light illumination. The quasi-solid state cells exhibit transient behavior similar to cells with liquid electrolyte suggesting that ion transport in the polymer gel electrolyte does not inherently influence the performance of these cells. Preliminary results under extended illumination suggest that the long term stability of the gel electrolyte cells is similar to that of liquid electrolyte cells. Optimization of the TiO₂/polymer gel interface should help to further increase the efficiency and stability of the cells.

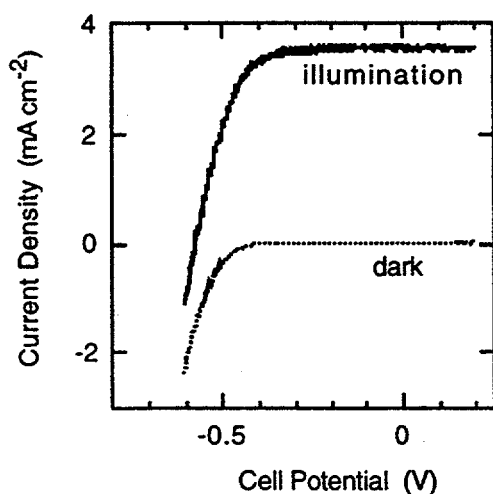


Figure 1. Current - voltage curves for a polymer gel electrolyte cell in the dark and under 30 mW cm⁻² white light illumination. The curves were obtained in a two electrode arrangement at a scan rate of 5 mV s⁻¹.

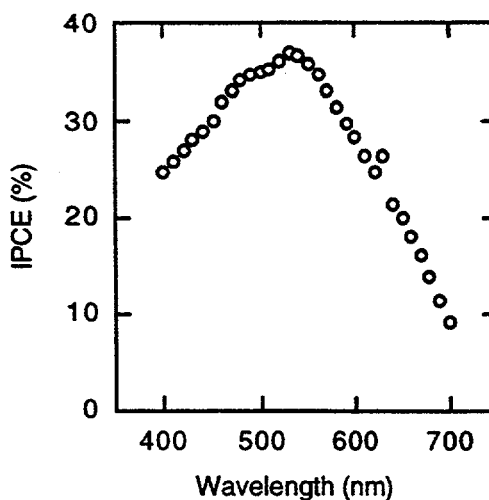


Figure 2. Incident Photon to Current Conversion Efficiency (IPCE) of a polymer gel electrolyte cell versus wavelength.

Electron Transport in Porous Nanocrystalline TiO₂ Photoelectrochemical Cells

Many recent innovations in photoelectrochemical solar energy conversion have been based on the use of porous nanocrystalline films [1-5]. These films are usually comprised of a three dimensional network of interconnected nanometer sized particles and exhibit many unique optical and electrical properties in comparison to planar single crystal or polycrystalline films. Nanometer sized particles are generally too small to sustain significant electric fields so that charge separation must be achieved by some other means. In one approach, sub-bandgap illumination may be used to excite dye molecules attached to the surface of the particles. The excited state of the dye molecule injects an electron into the particle and the dye is regenerated by an electron donor in the solution. Minority carriers are not involved in this process so that electrons may be collected with high efficiency as long as recombination in the form of electron transfer to an electron acceptor in the solution or to the oxidized form of the dye can be minimized. Dye sensitized, nanoporous TiO₂ photoelectrochemical cells are an example of this

approach and remarkably high energy conversion efficiencies have been achieved [1]. Another unique property of porous nanocrystalline films compared to single crystal materials is the high surface area. This is an important feature for the dye sensitization approach since high dye coverage is critical to obtaining high absorption coefficients for the films and hence high conversion efficiencies [1].

Previous studies on dye sensitized TiO₂ photoelectrochemical cells have shown that the photocurrent transient response is relatively slow with time constants on the order of milliseconds to seconds [6,7]. In contrast, the rate of electron injection into the TiO₂ electrode from the excited state of the dye molecule is a very fast process with time constants on the order of 10⁻⁹ s or smaller [8]. As a result, the transient response of devices based on porous nanocrystalline films is expected to be dominated by electron transport through the particle network. We have performed photocurrent transient measurements and Intensity Modulated Photocurrent Spectroscopy (IMPS) of dye sensitized porous nanocrystalline TiO₂ photoelectrochemical cells. We have shown that the transient response is dominated by electron transport in the film and can be explained by a diffusion model where the diffusion coefficient for electrons in the particle network is a function of the light intensity.

Figure 1 shows examples of photocurrent transients under monochromatic ($\lambda = 514$ nm) illumination at 0.05 mW cm⁻² and 4 mW cm⁻². At an illumination intensity of 0.05 mW cm⁻², the steady state photocurrent density was 6 μ A cm⁻² and the rise time was 60 ms. The rise time $t_{1/2}$ is defined by the time at which the current reaches half the steady state value. At very low light intensity the rise time was longer than 1 second. On increasing the light intensity, the rise time becomes progressively shorter, as can be seen in Figure 1b, which shows a photocurrent transient at 4 mW cm⁻² where the steady state photocurrent density is 0.4 mA cm⁻² and the rise time is 8 ms. At very high light intensities the transient response exhibits a subsequent decay due to diffusion limited transport of the redox couple in the electrolyte.

Figure 2 shows the steady state photocurrent and the maximum photocurrent plotted versus the incident light intensity. The maximum photocurrent is linear with the light intensity up to the highest light intensity in our experiments. The current maxima correspond to an incident photon to current conversion efficiency of about 20% through the whole light intensity range. This cell exhibits a threshold light intensity of about 10 mW cm⁻² below which the photocurrent maximum corresponds to the steady state value;

at higher light intensities the photocurrent rise is followed by a decay process due to limiting transport of the redox couple in the electrolyte. The threshold light intensity is an indicator of the optimum operational limit of the cell. A threshold light intensity of 10 to 50 mW cm⁻² was usually observed, which is slightly smaller than the solar intensity at AM 1, implying that the operation of these cells would be more efficient under diffuse sunlight.

Figure 3 shows a typical photocurrent rise at a light intensity of 4 mW cm⁻² on a semi-logarithmic plot. In this plot, a simple exponential rise would yield a straight line from which the time constant of the transient could be determined. The photocurrent rise, shown in Figure 3, is characterized by a fast component and a slow component illustrated by the two nearly linear regions in the plot. The linear region of the fast component usually extends over more than one time constant in the semi-logarithmic plot showing that the transient response is dominated by the fast component. The rise time of the fast component was generally found to be from several times to an order of magnitude smaller than that of the slow component. We have shown that the two components are derived from diffusion controlled electron transport in the film.

Figure 4 shows that the rise times exhibit a power law dependence on light intensity with a slope of -0.7. The rise times ranged from milliseconds to seconds over a light intensity range of almost three orders of magnitude. The exponent varied from sample to sample but for all experiments was in the range -0.6 to -0.8. Similar results were obtained for cells with liquid electrolyte.

Carrier transport in the semiconductor film can be described by the continuity equation:

$$\frac{\partial n}{\partial t} = \frac{1}{e} \frac{\partial J}{\partial x} + G - R$$

where n is the electron density under illumination, J is current density in the film, and G and R are the carrier generation rate and recombination rate, respectively. In the dye sensitized porous TiO₂ film, the generation rate can be written as $G = \Gamma \alpha \exp(-\alpha x)$, where Γ is the photon flux and α is the wavelength dependent absorption coefficient of the dye sensitized film. This implies that the dye concentration is uniform throughout the film. Recombination is assumed to be proportional to the electron concentration and can be written as $R = \frac{n - n_0}{\tau_0}$

where n_0 is the electron density in the dark and τ_0 is the position independent electron lifetime.

Due to the small particle size, carrier migration can be neglected. Assuming that the current density is dominated by diffusion the continuity equation becomes:

$$\frac{\partial \left(D_0 \frac{n(x,t)}{n_0} \frac{\partial (n(x,t))}{\partial x} \right)}{\partial x} - \frac{\partial n(x,t)}{\partial t} - \frac{n(x,t) - n_0}{\tau_0} + \Gamma \alpha \exp(-\alpha x) = 0$$

where D_0 is the diffusion coefficient in the dark. The first two terms represent the electron flux and the change in electron concentration with time, respectively. The third term represents the recombination rate and is characterized by the time constant τ_0 . The fourth term is the rate of electron injection from the photoexcitation process.

A numerical solution for the continuity equation was obtained using a Forward Time Central Space (FTCS) algorithm. The parameter γ describes the absorbance of the film and is given by $\gamma = \alpha d$ where d is the film thickness. The term $\beta = \frac{\Gamma \alpha d^2}{n_0 D_0}$ and is proportional to the light intensity. Figure 1c shows calculated transients for $\alpha d = 10$ and $\alpha d = 3$. Note that $\alpha d = 10$ would be obtained for a 10 μm thick film with an absorption coefficient of 10^4 cm^{-1} . The β values of 1000 and 300, respectively, were chosen to give the same photon flux. The inset in Figure 3 shows these transients on a semi-logarithmic plot. For the case where $\alpha d = 10$, corresponding to strong absorption, the photocurrent rise is characterized by two components with the initial fast component extending over more than one time constant in the semi-logarithmic plot. These features are consistent with the experimental observations. For the case where $\alpha d = 3$, corresponding to a relatively weak absorption, the transition between the two processes is not as distinct. This is due to the fact that fewer electrons are injected in the vicinity of the back contact thus slowing down the fast component of the photocurrent rise, while more electrons are injected in the outer portion of the film thus speeding up the slow component.

Figure 6 shows the evolution of the electron concentration profiles, calculated from the continuity equation, for the transients shown in Figure 1c. The concentration profile during the fast part of the transient is characterized by a steady build-up of a concentration peak within a short distance of the back contact. In the slow process, the electron concentration in the outer

portion of the film builds up to the steady state concentration gradient. In the absence of recombination of electrons with acceptors in the electrolyte the concentration peak moves to the outer part of the film resulting in a monotonic distribution of electron density in the electrode with the outer part of the film having the highest electron concentration. For the case of relatively weak absorption in the film ($\alpha d=3$), the concentration peak is far away from the back contact and the initial increase of the peak is much less pronounced. These results show that the fast and slow components of the transients reflect the variation of absorption efficiencies of different dye sensitized TiO₂ films.

Figure 7 shows a logarithmic plot of the rise time, $t_{1/2}$, of the calculated transients as a function of the incident light intensity in terms of the dimensionless absorption coefficient γ and the dimensionless light intensity β . The rise times of the calculated transients exhibit a power law dependence on light intensity with a slope of -0.5, similar to the experimental results shown in Figure 4. At the low light intensity limit, the time constant reaches a plateau corresponding to the condition where $n \rightarrow n_0$ and $D \rightarrow D_0$. A low light intensity for the onset of the rise time plateau is an indicator of low dopant density in the film. Experimentally, this plateau was not observed and time constants longer than 1 s were seen at very low light intensities. These observations give an upper limit for the dark diffusion coefficient D_0 of 10^{-7} cm² s⁻¹ much smaller than the value for transport of free electrons in single crystal TiO₂. In addition, we obtain an upper limit for the product $n_0 D_0$ on the order of 10^9 cm⁻¹ s⁻¹.

The features of the simulation can be changed by further modifying the diffusion equation. The slope in Figure 7 is related to the concentration dependence of the diffusion coefficient and it can be shown that if $D \propto n^\eta$, then the slope is given by $-\eta/(1+\eta)$. A stronger concentration dependence of the diffusion coefficient will increase this slope corresponding to a stronger dependence of the photocurrent rise time on the light intensity.

Introducing a recombination term into the continuity equation has little effect on the fast component of the transient but suppresses the slow part since electrons in the outer part of the film will recombine before reaching the back contact and contributing to the current. In this case the slow process is removed from the transient behavior, resulting in an overall faster transient response and lower steady state current. The inclusion of the recombination term also leads to a peak in the steady state electron concentration profile in the film. The appearance of the slow part of the transient is itself indicative of a relatively long lifetime for electrons in these

films.

The IMPS response can be also calculated for the diffusion controlled transport model with $D \propto n$ ($\eta=1$). Figure 5b shows a complex plane plot of the IMPS spectrum calculated for $\alpha d=10$ revealing two relaxation processes corresponding to the fast and slow components seen in the both the experimental and calculated photocurrent transients. The time constant associated with the imaginary maximum corresponds to the fast component while the time constant associated with the lower frequency semi-circle is associated with the slower component. For the case of strong absorption ($\alpha d=10$) the two processes are clearly seen in the complex plane plot. The complex plane IMPS spectrum obtained for $\alpha d=3$ at the same light intensity, Figure 5c, shows that the difference between the time constants of the two components becomes smaller when the absorption depth becomes sufficiently large. Experimentally, the separation between the two processes is not clearly distinguishable as seen in Figure 5a. The calculations presented here show two limiting cases and are not intended to give the best fit of the experimental data.

The time constant obtained from the frequency at the imaginary maximum for $\alpha d = 10$ decreases as the light intensity increases, as shown in Figure 7. The time constant from the calculated IMPS response is shorter than the calculated transient rise time consistent with the experimental observation shown in Figure 3. In the transient measurements, an electron concentration gradient has to be built up from the dark electron density in the film, which makes the photocurrent rise a rather slow process. In the IMPS measurement, the existing steady state electron concentration increases the diffusion coefficient, leading to a smaller time constant in the IMPS measurement.

In summary, the photocurrent transients observed for dye sensitized nanoporous TiO_2 films are relatively slow. Under backside illumination, the photocurrent rise is characterized by a fast component due to injection of carriers close to the contact and a slow component related to the build-up of the electron concentration gradient in the film to a steady state value. The fast component dominates the transient response and extends over more than one time constant on a semi-logarithmic plot. The rise time of the photocurrent transient exhibits a power law dependence on light intensity with an exponent of -0.6 to -0.8. The time constants obtained from IMPS measurements exhibit the same dependence although the values were smaller than those obtained from transient measurements at the same light intensity. The essential features

of the nonsteady state response can be described by a diffusion model where the electron diffusion coefficient is dependent on light intensity. Physically, this model is consistent with an electron transport process controlled by thermal excitation from trap states in the particles. We emphasize that the diffusion coefficient D is expected to be a function of the sample morphology and preparation methods. Finally, we note that this model can also be applied to porous nanocrystalline electrodes without dye sensitization, provided that the photogenerated holes are removed rapidly.

References

1. B. O'Regan and M. Grätzel, *Nature* 353, 737 (1991).
2. G.J. Meyer and P.C. Searson, *Interface* 2, 23 (1993).
3. F. Cao, G. Oskam, P.C. Searson, J.M. Stipkala, T. A. Heimer, F. Farzad, and G.J. Meyer, *J. Phys. Chem.* 99, 11976 (1995).
4. G. Hodes, I.D.J. Howell, and L.M. Peter, *J. Electrochem. Soc.* 139, 3136 (1992).
5. T.A. Heimer, C.A. Bignozzi, and G.J. Meyer, *J. Phys. Chem.* 97, 11987 (1993).

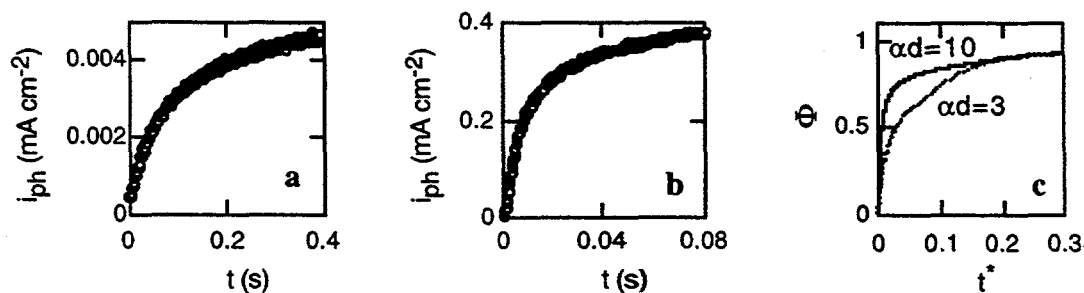


Figure 1. Photocurrent transients recorded under monochromatic (514 nm) illumination at a light intensity of (a) 0.05 mW cm^{-2} and (b) 4 mW cm^{-2} . The TiO_2 electrodes were biased at 0 V. (c) Photocurrent transients calculated according to equation {4} for $\alpha d=10$ and $\alpha d=3$. The values for β used in the calculation were 1000 and 300, respectively, and were chosen to correspond to the same light intensity. The abscissa is dimensionless time t^* defined by $t^* = \frac{D_0 t}{d^2}$ and the ordinate is the quantum efficiency Φ . Recombination is neglected in the calculation ($\tau_0 \rightarrow \infty$).

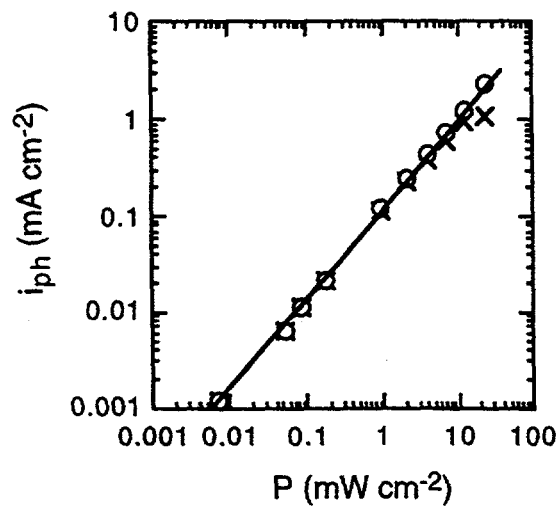


Figure 2. The photocurrent maximum (o) and the steady state photocurrent (x) plotted versus monochromatic (514 nm) light intensity. The TiO_2 electrodes were biased at 0 V.

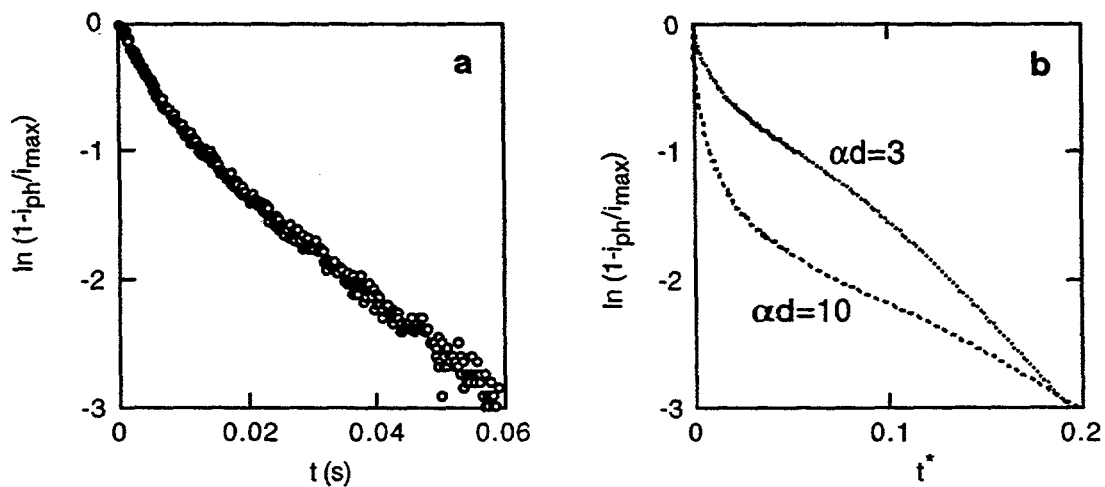


Figure 3. (a) Semi-logarithmic plot of a photocurrent transient under monochromatic (514 nm) illumination at 4 mW cm^{-2} . (b) Semi-logarithmic plot of the calculated photocurrent transients from Figure 1(c).

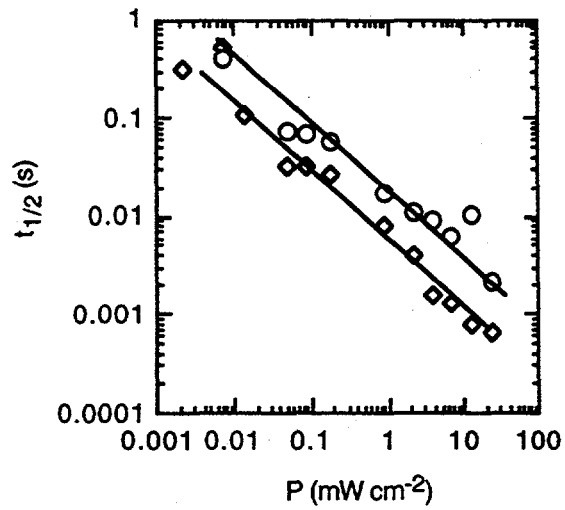


Figure 4. The photocurrent rise time (o) and IMPS time constant (\diamond) of a TiO_2 cell biased at 0 V versus the monochromatic (514 nm) light intensity.

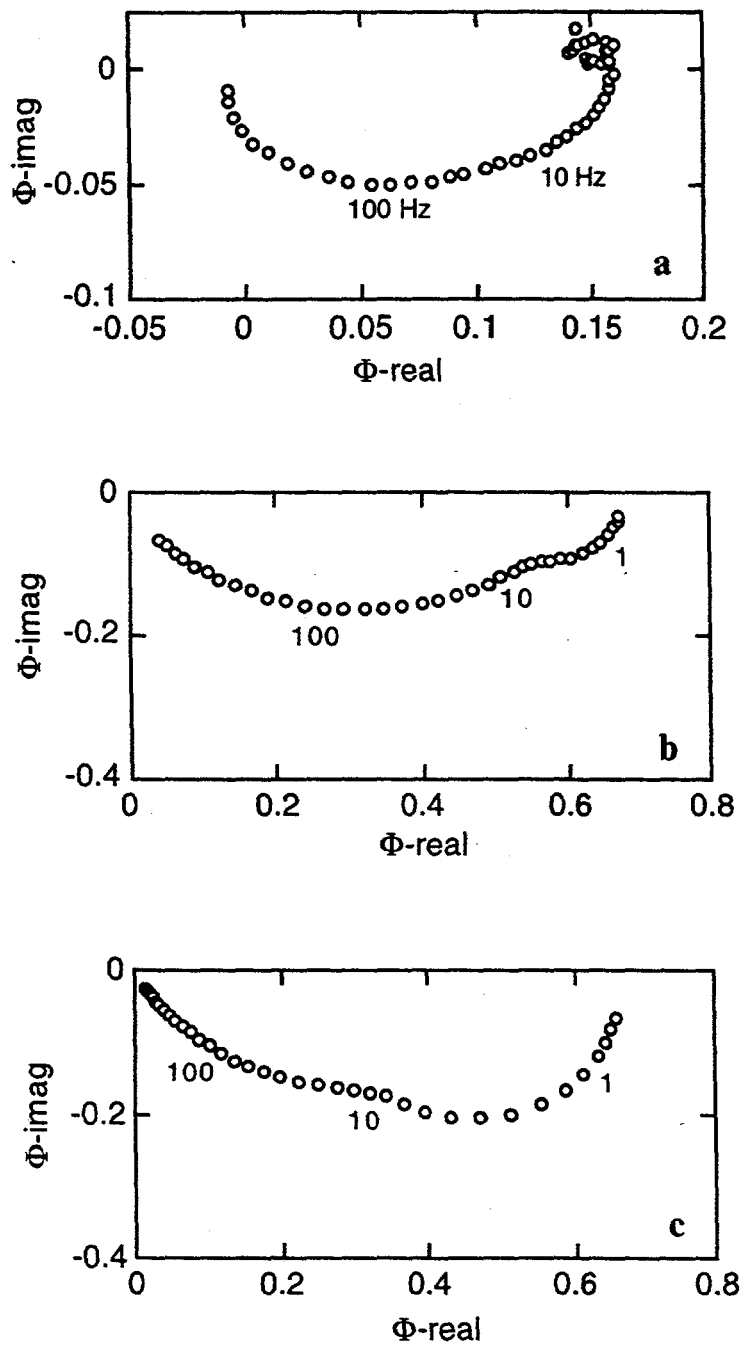


Figure 5. (a) Complex plane plot of the IMPS response of a TiO_2 cell at a base light intensity of 4 mW cm^{-2} . Complex plane IMPS response calculated according to equation {4} (see Appendix C) for (b) $\alpha d=10$ and $\beta=1000$ and (c) $\alpha d=3$ and $\beta=300$. In (b) and (c) the frequencies are in dimensionless units.

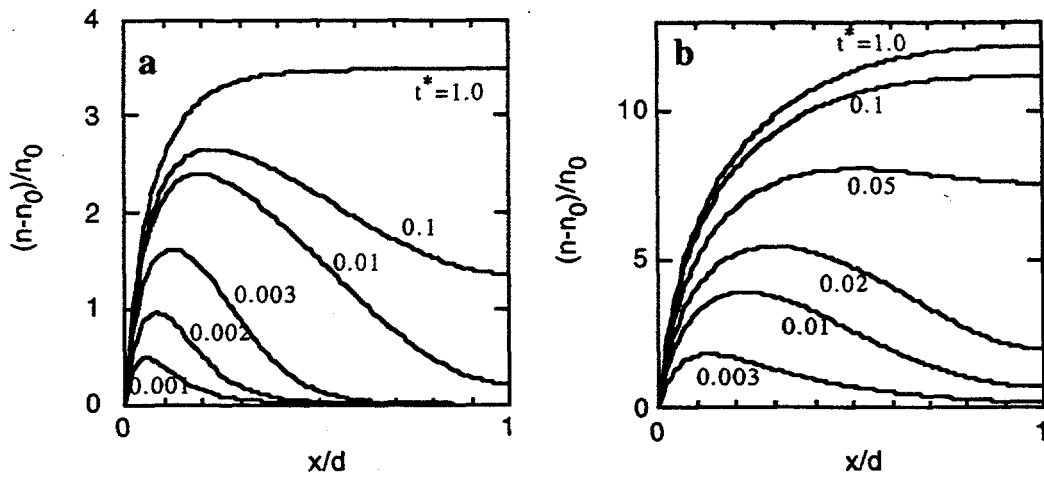


Figure 6. Calculated spatial distribution of the electron concentration in the film obtained from equation {4} as a function of dimensionless time t^* for (a) $\alpha d=10$, $\beta=1000$ and (b) $\alpha d=3$, $\beta=300$.

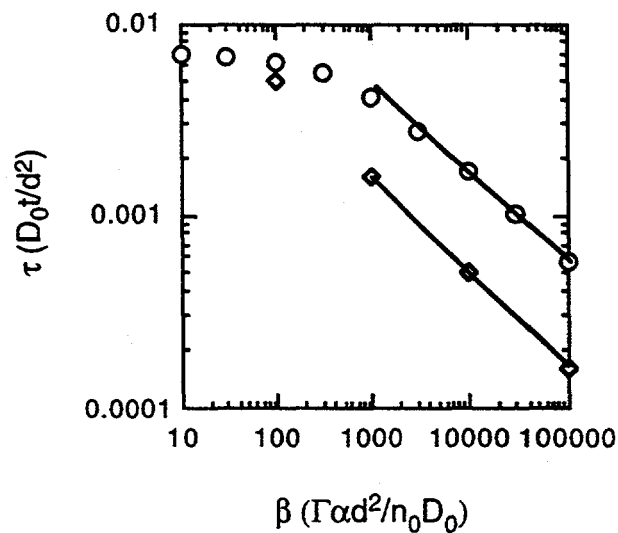


Figure 7. Dimensionless photocurrent rise times (o) and IMPS time constants (◇) calculated from equation {4} plotted versus β . For all calculations $\alpha d=10$.

Optical Properties of Nanostructured TiO₂ Films

Structurally the TiO₂ films are highly porous and are comprised of an interconnected network of nanometer size particles. The photoaction spectra display a small but significant sub-band gap response indicative of intraband gap states. The films are electrochromic and turn a uniform black color at negative potentials more than -0.4 V (SSCE). The attenuation increases as the potential is scanned in the negative direction and reaches a plateau that is dependent on the film thickness, showing that the coloration occurs throughout the film. In thinner films, the apparent absorption edge shifts to higher energy with negative applied bias, as has been described previously.

Figure 1 shows typical voltammograms for a TiO₂ film as a function of scan rate. At positive potentials the anodic current is very small, less than 1 $\mu\text{A cm}^{-2}$ at 0.5 V (SSCE). On scanning the potential more negative the cathodic current increases steadily and if the potential is scanned more negative than -0.4 V an anodic peak is observed on the reverse scan. This peak is not observed in the voltammogram for the conductive glass substrate in the same solution. The peak anodic current is proportional to the square root of the scan rate.

Figure 2 shows a plot of the reoxidation charge versus the attenuation of the film. The attenuation data were recorded at the negative scan limit of the cyclic voltammogram and the reoxidation charge was calculated by integration of the corresponding anodic peak. This plot shows that the attenuation of the film is directly correlated to the charge involved in the process.

The appearance of a dark blue-black color on heated, irradiated, or electrochemically reduced TiO₂ is extremely well documented over the last several decades [1-3]. The absorption spectra are generally broad and display maxima in the visible or infra red region. The color change has been generally attributed to Ti(III) states and there now exists a large body of spectroscopic evidence to support this assignment. Perhaps the most detailed studies were performed by Von Hippel and co-workers [2] who explored the optical properties of single crystal rutile materials. At temperatures above 900 °C the absorption increased through the visible and beyond 4 μm and was assigned to free electrons in a 3d-conduction band. Extensive reduction of the crystal resulted in a room temperature discoloration with an absorption maximum at 1500 nm assigned to Ti(III) traps in various surroundings. Therefore, the attenuation data reported here for porous nanocrystalline TiO₂ films support the presence of Ti(III) states. The high attenuation seen at negative potentials indicates that there is a very high

density of these states. Further evidence for the presence of Ti(III) states is the appearance of an EPR absorption on electrochemically reduced films. The g factor of 1.903 is in good agreement with results from other titania materials excited with band gap light where similar spectra were obtained and assigned to Ti(III) trap states [4-6]. To our knowledge, these data represent the first observation by EPR that electrochemical reduction of TiO_2 leads to the formation of Ti(III) states.

References

1. F.A. Grant, *Rev. Modern Phys.* 31, 646 (1959).
2. A. von Hippel, J. Kalnjas, and W.B. Westphal, *J. Phys. Chem. Solids* 23, 779 (1962).
3. N.M. Dimitrijevic, D. Savic, O.I. Micic, and A.J. Nozik, *J. Phys. Chem.* 88, 4278 (1984).
4. T. Huizinga and R. Prins, *J. Phys. Chem.* 85, 2156 (1981).
5. R.F. Howe and M. Grätzel, *J. Phys. Chem.* 94, 2566 (1990).
6. O.I. Micic, Y. Zhang, K.R. Cromack, A.D. Trifunac, and M.C. Thurnauer, *J. Phys. Chem.* 97, 7277 (1993).

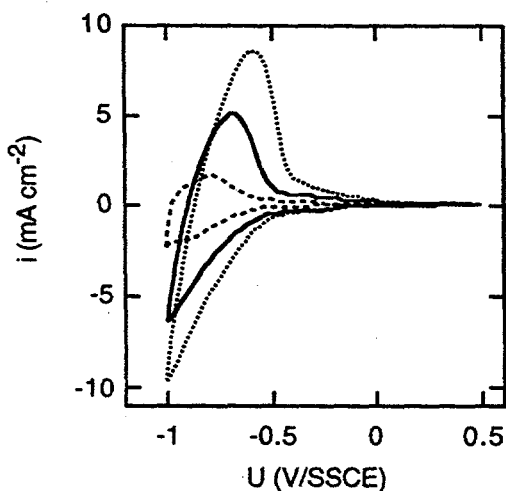


Figure 1. Charge under the anodic peak plotted against the attenuation as a function of the negative scan limit in the range -0.4 to -1.0 V (SSCE).

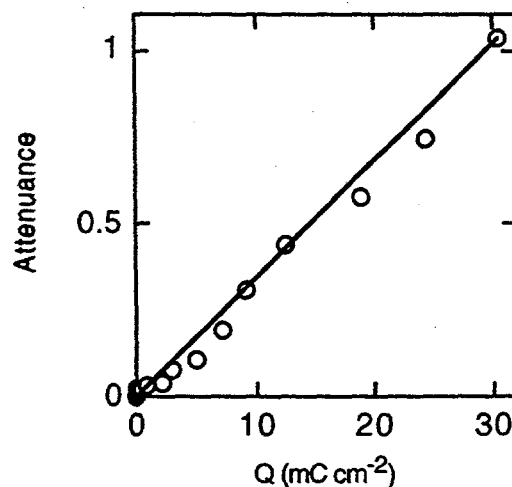


Figure 2. Cyclic voltammograms for a TiO_2 electrode in 0.1 M Na_2SO_4 at pH 2 as a function of scan rate.

Electrical Properties of TiO₂ Films

We have measured the photoconductivity of nanoparticle TiO₂ films deposited onto lithographically patterned interdigitated electrode arrays. Figure 1 shows a current - voltage curve for a 1 μm thick film of 200 nm particles prepared from a colloid aged at 200°C. The interdigitated electrode array was fabricated with two sets of 15 μm wide gold fingers at 15 μm spacings. These films are rectifying and current flow only occurs at breakdown voltages on the order of 10⁴ V cm⁻¹. The transient response of these junctions is very slow, as shown in Figure 2, and dependent on light intensity and temperature.

The diffusion coefficient for electrons in the film does not correspond to the transport of free electrons in the conduction band of single crystal TiO₂. Based on an electron mobility of about 1 cm² V⁻¹ s⁻¹ for single crystal TiO₂ [1] the diffusion coefficient for free electrons determined to be on the order of 10⁻² cm² s⁻¹ at room temperature, much larger than the values implied from the slow transients. From the experimental measurements, we estimate a value of 4 x 10⁷ cm⁻¹ s⁻¹ for the product n₀D₀ and using the Einstein relation to correlate the mobility and diffusion coefficient, a dark conductivity (σ = neμ₀) for the TiO₂ films is calculated to be in the order of 10⁻⁹ W⁻¹ cm⁻¹. A dark conductivity of this order of magnitude has been reported in the literature for the porous nanostructured TiO₂ films [2].

These results imply that the diffusion coefficient represents the thermally activated transport of electrons through the particle network. In this case the diffusion coefficient of electrons in the films is expected to be dependent on the illumination intensity and the particle size in the TiO₂ film, results that we have confirmed experimentally. Similar effects have been reported in amorphous and disordered semiconductors where charge trapping can give rise to very slow phototransient processes [3,4]. These materials are characterized by a high density of trap sites and, consequently, charge transport is often dominated by the properties of the traps. In many cases the traps are distributed over a broad energy range so that the electron mobility is dependent on trap occupancy (Fermi level) and hence on the electron density. Another example involves polycrystalline CdS and CdSe films fabricated from sintered powders. These films are characterized by high conductivity particles separated by photosensitive, low-conductivity contact regions [5]. On illumination, the resistance of the contact regions may be reduced resulting in an increase in the electron mobility and hence the current density.

References

1. F. Cao, G. Oskam, P.C.Searson, J.M. Stipkala, T.A. Heimer, and G.J. Meyer, *J. Phys. Chem.* 99, 11974 (1995).
2. M.A. Rashti and D.E. Brodie, *Thin Solid Films* 240, 163 (1994).
3. K. Schwarzburg and F. Willig, *Appl. Phys. Lett.* 58, 2520 (1991).
4. F.W. Schmidlin, *Phys. Rev.* 16, 2362 (1977).
5. R.H. Bube, *Photoconductivity of Solids*, Robert Krieger Publishing Company, New York (1978).

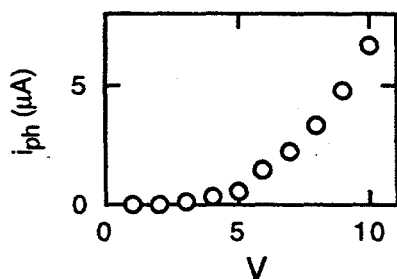


Figure 1. I-V curve for a Au-TiO₂-Au junction fabricated by deposition of 200 nm TiO₂ particles on an interdigitated electrode array. Current was recorded after 5 minutes stabilization at an illumination intensity of 4 mW cm⁻².

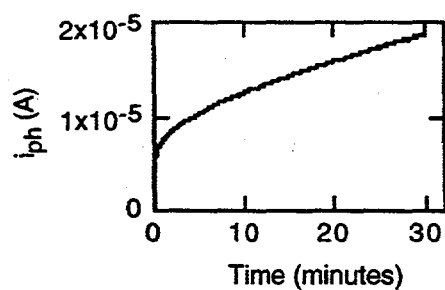


Figure 2. Photocurrent transient for a Au-TiO₂-Au junction at a bias of 10 V at an illumination intensity of 4 mW cm⁻².

Publications Acknowledging NREL Support

Photoelectrochemical Solar Energy Conversion at Nanostructured Materials. Meyer, G.J.; Searson, P.C. *Interface: J. Electrochem. Soc.* 1993, 2, 23-27.

Molecular Level Photovoltaics: The Electro-Optical Properties of Metal Cyanide Complexes Anchored to Titanium Dioxide. Heimer, T.A.; Bignozzi, C.A.; Meyer, G.J. *J. Phys. Chem.* 1993, 97, 11987-11994.

Enhanced Spectral Sensitivity from Ru(II) Polypyridyl Photovoltaic Devices. Argazzi, R.; Bignozzi, C.A.; Heimer, T.A.; Castellano, F.N.; Meyer, G.J. *Inorg. Chem.* 1994, 33, 5741-5749.

Optical and Electrical Properties of Nanostructured Titanium Dioxide Films. Cao, F.; Oskam, G.; Searson, P.C.; Stipkala, J.; Farzad, F.; Heimer, T.A.; Meyer, G.J. *J. Phys. Chem.* 1995, 99, 11974-11980.

Efficient Ruthenium Diimine Modified Nanocrystalline TiO₂ Photoanodes. Heimer, T.A.; Meyer, G.J. *Proc. Electrochem. Soc.* 1995, 121, 189-197.

Electron Injection Rates in Sensitized Nanostructured TiO₂ Photovoltaic Devices. Heimer, T.A.; Meyer, G.J. *Proc. Electrochem. Soc.* 1995, 121, 167-179.

A Solid State, Dye Sensitized Photoelectrochemical Cell. Cao, F.; Oskam, G.; Searson, P.C. *J. Phys. Chem.* 1995, 99, 17071.

A Quasi Solid State, Dye Sensitized TiO₂ Photoelectrochemical Cell. Cao, F.; Oskam, G.; Searson, P.C. *Proc. Electrochem. Soc.* 1995, 121, 180.

Photosensitization of Wide Bandgap Semiconductors with Antennae Molecules. Bignozzi, C.A.; Argazzi, R.; Schoonover, J.R.; Meyer, G.J.; Scandola, F. *Sol. Energy Mater. Sol. Cells* 1995, 38, 187-198.

Long-Lived Charge Separation Across Nanostructured TiO₂ Interfaces. Argazzi, R.; Bignozzi, C.A.; Heimer, T.A.; Castellano, F.N.; Meyer, G.J. *J. Am. Chem. Soc.* 1995, 117, 11815-11816.

An Acetylacetonate Based Semiconductor-Sensitizer Linkage. Heimer, T.A.; D'Arcangelis, S.T.; Farzad, F.; Stipkala, J.M.; Meyer, G.J. *Inorg. Chem.* 1996, 35, 5319-5324.

Luminescence of Charge Transfer Sensitizers Anchored to Metal Oxide Nanoparticles. Heimer, T.A.; Meyer, G.J. *J. Lumin.* 1996, 70, 468-478.

Electron Transport Properties in Porous Nanocrystalline TiO₂ Photoelectrochemical Cells. Cao, F.; Oskam, G.; Searson, P.C.; Meyer, G.J. *J. Phys. Chem.* 1996, 100, 17021-17027.

Light Induced Processes in Molecular Gel Materials. Castellano, F.N.; Meyer, G.J. *Prog. Inorg. Chem.* 1997, 44, 167-209.

Remote Electron Injection from Supramolecular Sensitizers. Argazzi, R.; Bignozzi, C.A.; Heimer, T.A.; Meyer, G.J. *Inorg. Chem.* 1997, 36, 2-3.

Light Induced Charge Separation Across Ru(II) Modified Nanocrystalline TiO₂ Interfaces with Phenothiazine Donors. Argazzi, R.; Bignozzi, C.A.; Heimer, T.A.; Castellano, F.N.; Meyer, G.J. *J. Phys. Chem. B* 1997, 101, 2591-2597.

Efficient Light-to-Electrical Energy Conversion: Nanocrystalline TiO₂ Films Modified with Inorganic Sensitizers. Meyer, G.J. *J. Chem. Ed.* 1997, 74, 652-656.

Electron Transfer Kinetics in Sensitized TiO₂ Photoelectrochemical Cells. Meyer, G.J. *American Institute of Physics Conference Proceedings 404: Future Generation Photovoltaic Technologies 1997*, 404, 137-144.

The Open Circuit Photovoltage in Dye Sensitized Nanostructured TiO₂ Films. Cao, F.; Oskam, G.; Searson, P.C. in *Proceedings of the 3rd International Meeting on New Trends in Photoelectrochemistry*, 1997.

Light Induced Charge Separation at Sensitized Sol-Gel Processed Semiconductors. Stipkala, J.M.; Heimer, T.A.; Livi, K.J.T.; Meyer, G.J. *Chem. Mater.* 1997, 9, 2341-2353.

Intercomponent and Interfacial Electron Transfer Processes in Polynuclear Metal Complexes Anchored to Transparent TiO₂ Films. Bignozzi, C.A.; Argazzi, R.; Indelli, M.T.; Scandola, F.; Schoonover, J.R.; Meyer, G.J. *Sol. Energy Mater. Sol. Cells*, in press.

REPORT DOCUMENTATION PAGE

Form Approved
OMB NO. 0704-0188

Public reporting burden for this collection of information is estimated to average 1 hour per response, including the time for reviewing instructions, searching existing data sources, gathering and maintaining the data needed, and completing and reviewing the collection of information. Send comments regarding this burden estimate or any other aspect of this collection of information, including suggestions for reducing this burden, to Washington Headquarters Services, Directorate for Information Operations and Reports, 1215 Jefferson Davis Highway, Suite 1204, Arlington, VA 22202-4302, and to the Office of Management and Budget, Paperwork Reduction Project (0704-0188), Washington, DC 20503.

1. AGENCY USE ONLY (Leave blank)	2. REPORT DATE July 1998	3. REPORT TYPE AND DATES COVERED Final Report	
4. TITLE AND SUBTITLE Solar Energy Conversion at Dye-Sensitized Nanostructured Electrodes Fabricated by Sol-Gel Processing		5. FUNDING NUMBERS C: XAD-3-12114-04 TA: PV802803	
6. AUTHOR(S) P.C. Searson and G.J. Meyer		8. PERFORMING ORGANIZATION REPORT NUMBER	
7. PERFORMING ORGANIZATION NAME(S) AND ADDRESS(ES) The Johns Hopkins University Baltimore, MD 21218		10. SPONSORING/MONITORING AGENCY REPORT NUMBER SR-520-24521	
9. SPONSORING/MONITORING AGENCY NAME(S) AND ADDRESS(ES) National Renewable Energy Laboratory 1617 Cole Blvd. Golden, CO 80401-3393		11. SUPPLEMENTARY NOTES NREL Technical Monitor: R. McConnell	
12a. DISTRIBUTION/AVAILABILITY STATEMENT		12b. DISTRIBUTION CODE	
13. ABSTRACT (<i>Maximum 200 words</i>) The significant achievements accomplished in this program include <ul style="list-style-type: none"> •the first demonstration of osmium polypyridyl compounds as sensitizers •the first demonstration of donor-acceptor compounds as sensitizers •the first use of alternative acac-based sensitizer-semiconductor linkages •the first demonstration of "remote" interfacial electron transfer •the first application of bimetallic compounds as sensitizers •the first correlation of the interfacial charge recombination rate constant with the open-circuit photovoltage in sensitized materials •the first demonstration of a solid-state dye-sensitized TiO₂ cell •an alternative band-edge unpinning model for the nanocrystalline TiO₂/electrolyte interface at negative applied potentials, •the first self-consistent model of electron transport in dye-sensitized TiO₂ films. 			
14. SUBJECT TERMS photovoltaics ; solar energy conversion ; sensitizers ; nanostructured electrodes ; sol-gel processing ; dye-sensitized photoconversion		15. NUMBER OF PAGES 28	16. PRICE CODE
17. SECURITY CLASSIFICATION OF REPORT Unclassified	18. SECURITY CLASSIFICATION OF THIS PAGE Unclassified	19. SECURITY CLASSIFICATION OF ABSTRACT Unclassified	20. LIMITATION OF ABSTRACT UL